Research Square

Preprints are preliminary reports that have not undergone peer review. They should not be considered conclusive, used to inform clinical practice, or referenced by the media as validated information.

Tunable sliding ferroelectricity and magnetoelectric coupling in two-dimensional multiferroic MnSe materials

Mingwen Zhao (✉ zmw@sdu.edu.cn)
Shandong University
Kehan Liu
Shandong University
Xikui Ma
Shandong University
Shuoke Xu
Shandong University
Yangyang Li
Shandong University https://orcid.org/0000-0003-4469-0659

Article

Keywords:

Posted Date: July 27th, 2022

DOI: https://doi.org/10.21203/rs.3.rs-1853018/v1

License: This work is licensed under a Creative Commons Attribution 4.0 International License.
Read Full License

Tunable sliding ferroelectricity and magnetoelectric coupling in two-dimensional multiferroic MnSe materials

Kehan Liu, Xikui Ma, Shuoke Xu, Yangyang Li, Mingwen Zhao*

School of Physics, Shandong University, Jinan 250100, China

ABSTRACT: Sliding ferroelectricity (SFE) found in two-dimensional (2D) van der Waals (vdW) materials, such as BN and transition-metal dichalcogenides bilayers, open an avenue for 2D ferroelectric materials. The multiferroic coupling in 2D SFE materials is expected to bring about new concepts for spintronic memory devices. Here, using first-principles calculations, we demonstrate that the recently-synthesized MnSe multilayers [ACS Nano 15, 13794 (2021)] have large reversible out-of-plane electric polarization (~10.6 pC/m) and moderate interlayer sliding barriers superior to the existing 2D SFE materials. More interestingly, the intrinsic electric polarization is also accompanied by nonzero net magnetic moments whose direction is dependent on the electric polarization direction and thus can be switched by interlayer sliding. Additionally, both the SFE and magnetoelectric coupling can be effectively regulated by external strain and/or hole doping. Our findings suggest the potential of MnSe multilayers in 2D multiferroic and spintronic applications.

INTRODUCTION

Ferroelectric materials have switchable bistable states with opposite spontaneous electric polarization that can be reversed via external electric field, enabling application in non-volatile memory devices[1]. The traditional ferroelectric materials, such as perovskite oxide $PbTiO_3$,[2] $BaTiO_3$,[3] and $BiFeO_3$ [4,5] where the electric polarization originates from the displacement of octahedral center ion are facing many challenging in miniaturization and integration of nanoelectronics device, due to interface distortion and depolarization field[6,7]. The emergency of two-dimensional (2D) van der Waals (vdW) ferroelectric materials with atomic thickness and clean interface, such as IV-VI group compounds[8-10], $CuInP_2S_6$[11,12] and In_2Se_3[13,14] extends the border of ferroelectricity to the few atomic layers. However, the 2D ferroelectric materials which have been achieved in experiments under ambient conditions remain rare due to the restrictions of structural symmetry and stability.

Sliding ferroelectricity (SFE) found in 2D vdW bilayers where the out-of-plane electric polarization can be switched by lateral sliding between the two monolayers[15-17] opens a fascinating avenue for the study of 2D ferroelectricity. The electric polarization in these 2D vdW ferroelectric materials stems from the interlayer charge distribution and thus has the dependence on the stacking pattern and twisting angle of the two monolayers[15-17], offering abundant approaches to tune the ferroelectricity. To date, the SFE under room temperature has been observed in twisting layers of hexagonal boron nitride (BN)[18-20] and transition-metal dichalcogenides (TMDs)[21-23] and untwisted heterobilayers of TMDs[24]. However, the electric polarization of the SFE materials is much weaker than that of the traditional ferroelectric materials. For example, the electric polarization of MoS_2 and WTe_2 are only 0.97 pC/m [25] and 0.38

pC/m [26], respectively. Improving the electric polarization of the SFE materials is quite crucial for the relevant functional device application.

Additionally, the coupling of different ferroic orders (such as ferroelectricity, ferromagnetism and ferroelasticity) in multiferroic materials is essential for information processing and memory devices[27]. In particular, magnetoelectric coupling[28-30] where magnetism can be regulated by electric field is promising for the electric-writing and magnetic-reading devices. The emergency of SFE in 2D vdW materials brought about a fascinating mechanism of magnetoelectric coupling that differs from the conventional multiferroics[29,31-33]. For example, the magnetoelectric coupling in the multiferroic bilayer VS_2 consisting of two ferromagnetic (FM) monolayers via interlayer sliding has been predicted.[33] However, the layered VS_2 materials have yet been synthesized in experiments. Compared to ferromagnets, antiferromagnetic (AFM) materials have the advantages of faster spin dynamics and low sensitivity to stray magnetic fields, which are ideal for spintronic memory devices[34]. Therefore, searching for a 2D AFM materials with remarkable SPE and magnetoelectric coupling is of great significance for achieving the SPE-controlled magnetism and relevant device applications.

Here, by means of first-principles calculations we demonstrate the SFE and magnetoelectric coupling in the antiferromagnetic 2D vdW MnSe bilayer and multilayers which have been synthesized in recent experiments[35]. Our computations show MnSe bilayer has stronger electric polarization than BN and other vdW SFE bilayers accompanied by remarkable magnetoelectric coupling. The electric polarization of MnSe multilayers is stronger than that of MoS_2 and WTe_2 by more than one order. Moreover, the electric polarization and magnetism can be significantly regulated by applying external strain and/or hole doping. The tunable ferroelectricity

and magnetoelectric coupling of the 2D vdW MnSe materials offer a promising platform for study of sliding multiferroics and relevant spintronics device applications.

RESULTS AND DISCUSSION

1. Sliding ferroelectricity in MnSe bilayer

The lattice structure of MnSe monolayer is composed of two buckled honeycomb MnSe sublayers which are linked together by Mn-Se bonds[35], as shown in Fig. 1a. The Mn/Se atoms of the upper sublayer reside alternatively atop the Se/Mn atoms of the lower sublayer. Each unit cell contains two Mn atoms and two Se atoms with the lattice constant of 4.28 Å, which belongs to the space group of P-3m1. The lengths of the Mn-Se bonds are respectively 2.58 (within MnSe sublayer) and 2.59 (between MnSe sublayers) Å. The height of the bucked MnSe sublayer determined from the distance between Mn and Se atomic layers is about 0.73 Å. Although each buckled MnSe sublayer has out-of-plane electric polarization, the two MnSe sublayers of the centrosymmetric MnSe monolayer have opposite buckling, whose electric polarization cancel each other out. This feature enables us to recover the electric polarization of MnSe bilayer by breaking the equivalence of the two MnSe sublayers.

Our DFT calculations also showed that MnSe monolayer has an AFM ground state which is energetically more favorable than the ferromagnetic (FM) state by about 0.4 eV per unit cell, in good consistence with the previous work[35]. The AFM state contains two FM MnSe sublayers which are coupled antiferromagnetically, and the magnetic moments of each FM sublayer mainly stem from the 3d electrons of Mn atoms with the in-plane easy magnetization direction. The electronic band structure and orbital-resolved electron density of states of MnSe monolayer are depicted in Fig. 1b, which indicate the semiconducting characteristics with an indirect band gap (Γ-K) of 1.72 eV

and a direct band gap (Γ-Γ) of 2.05 eV. The valence band maximum (VBM) is contributed by the 3p orbitals of Se and 3d orbitals of Mn, while the conduction band minimum (CBM) is mainly contributed by the 3d orbital of Mn. Further analysis reveals that the electronic occupied states near the Fermi level stem mainly from the $3p_x/p_y$ orbitals of Se and $3d_{xy}/d_{x^2-y^2}$ orbitals of Mn atoms, as shown in Fig. S1 of the Supplementary materials. The hybridization between the 3p orbitals of Se and 3d orbitals of Mn atom is remarkable for the valence bands near the Fermi level, which contributes to the unique SFE and magnetoelectric coupling of MnSe bilayer as discussed in the following section.

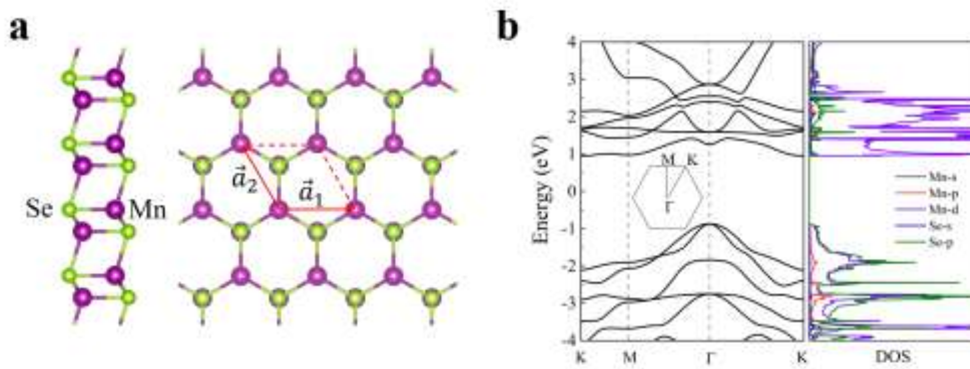

Fig. 1 Atomic configuration and electronic structure of MnSe monolayer. a Top and side view of MnSe monolayer, in which the unit cell is marked by red arrow and dashed line. The Mn and Se atoms are respectively represented by violet and green balls. **b** Band structure and projected density of states of MnSe monolayer, the first Brillouin zone is shown in the inset.

The inversion symmetry of the MnSe monolayer can be lifted by constructing a MnSe bilayer. We firstly scanned the stacking energy profile of a MnSe bilayer as upper monolayer sliding with respect to the down monolayer. Two energy minimal stacking patterns (denoted as AB and BA) are found in the energy profile which are energetically

degenerate, as shown in Fig. 2a. They are linked by an intermediate state (IS) locating in the middle of the sliding pathway. The double-wall potential profile hints the ferroelectricity of the MnSe bilayer. In terms of AB stacking pattern, the Mn atoms of the upper monolayer are right over the Se atoms of the down monolayer, while the Mn atoms of the down monolayer are right below the hexagonal center of the upper monolayer, as marked in Fig. 2c. Such interlayer inequivalence lifts the inversion symmetry and reduces the space group to p3m1. The electron redistribution due to the interlayer inequivalence leads to charge transfer between the two monolayers and thus out-of-plane electric polarization. The intrinsic electric polarization of the MnSe bilayer is further verified by electrostatic potential difference (~ 0.23 V) between the two monolayers, which is an order of magnitude larger than TMDs MX_2 (M = Mo, W; X = S, Se, Te)[36], as shown in Fig. 2c. Similar case can also be found in the BA stacking pattern, except the opposite charge transfer and electric polarization direction. Therefore, the electric polarization direction of the MnSe bilayer can be reversed by switching the stacking pattern between AB and BA via interlayer sliding, demonstrating the SEF characteristics of MnSe bilayer.

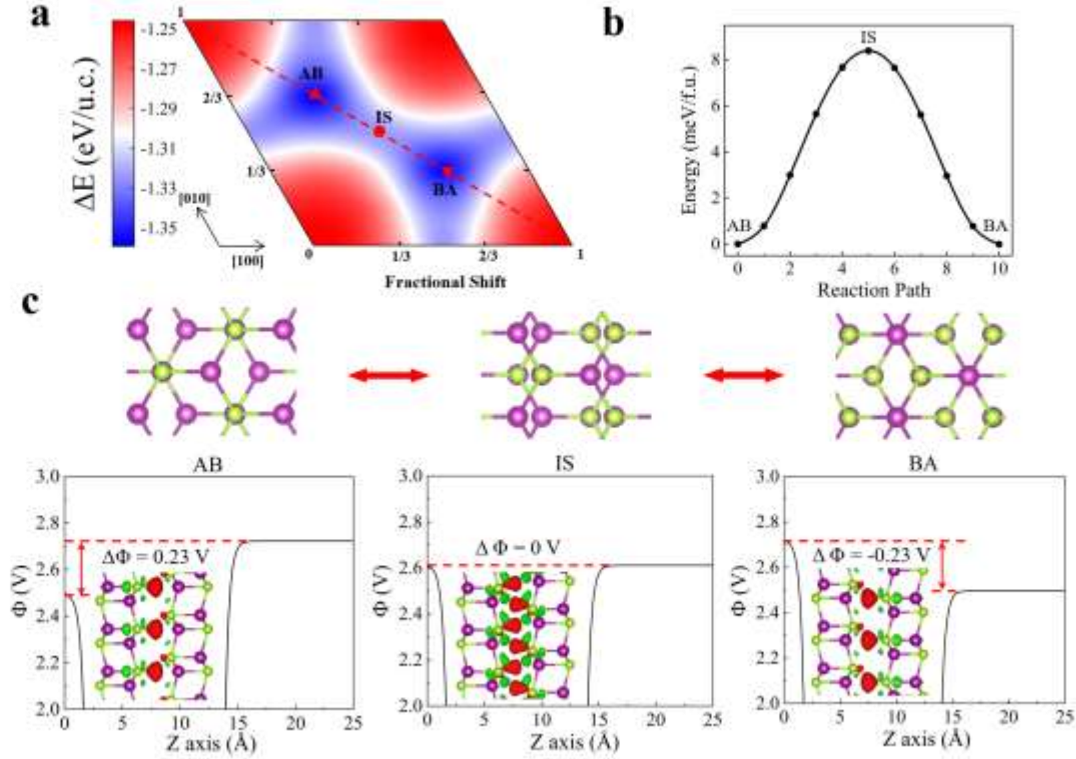

Fig. 2 Ferroelectric switching of MnSe bilayer via interlayer sliding. a The interlayer binding energy profile as a function of interlayer sliding for MnSe bilayer, in which the two energy degenerate stacking and intermediate state are denoted as AB, BA and IS, respectively. **b** Ferroelectric switching pathway of MnSe bilayer. **c** Top view and plane averaged electric potential of AB, IS and BA in MnSe bilayer. Insets are the corresponding side view and charge density difference, in which the red and green isosurfaces respectively indicate electron accumulation and depletion.

We further explored the possible ferroelectric switching path of MnSe bilayer through the nudge-elastic-band (NEB) method, as displayed in Fig. 2b. The energy barrier of interlayer sliding between AB and BA stacking is estimated to be 8.4 meV/f.u., which is much lower than those of $BiFeO_3$ (~ 430 meV/f.u.)[4] and In_2Se_3 (~ 60 meV/f.u.)[37] and comparable to that of BN (~ 4 meV/f.u.)[25], indicating the feasibility of ferroelectric switching and the stability of SPE of MnSe bilayer. Furthermore, as shown in Fig. 3a, the calculated variation of electric polarization in the interlayer sliding

process indicates that the vertical ferroelectric polarization for MnSe bilayer can reach 2.7 pC/m, which is larger than BN (~ 2.08 pC/m)[25] and WTe_2 (~ 0.38 pC/m)[26]. The enhanced electric polarization and moderate ferroelectric switching barrier verify the excellent SPE of MnSe bilayer.

2. Magnetoelectric coupling in antiferromagnetic MnSe multilayers

The electric polarization of the MnSe bilayer also induces the electron spin-splitting in the electronic band structures, which can be ascribed to the electron transfer between the two antiferromagnetic MnSe monolayers, as shown in Fig. 3a. For the AB stacking pattern, the electrons in the spin-down channel transfer from the upper Mn atoms to the lower Se atoms at the interface, as depicted in Fig. 3b, resulting in net magnetic moment of 8 mμ_B per unit cell. For the BA stacking pattern, the spin-up electrons transfer from lower Mn atom to upper Se atom at the interface, leading to the opposite net magnetic moment of 8 mμ_B per unit cell. Therefore, accompanied by the inversion of the electric polarization direction via interlayer sliding, the direction of the spin can also be switched, displaying the magnetoelectric coupling characteristics. This is also consistent with the variation of the electronic band structures of the two stacking patterns, as shown in Fig. 3c. The degeneracy of the two spin channels is lifted oppositely in the AB and BA stacking patterns, and the spin splitting is more remarkably near the Γ and K points. The spatial distributions of the charge density of the VBM at the Γ point reside mainly at one MnSe monolayer and interface Se atoms of the other MnSe monolayer, as shown in the insets of Fig. 3c. For the IS which is centrosymmetric, electric polarization and spin-polarization disappear simultaneously, verifying the characteristics of magnetoelectric coupling.

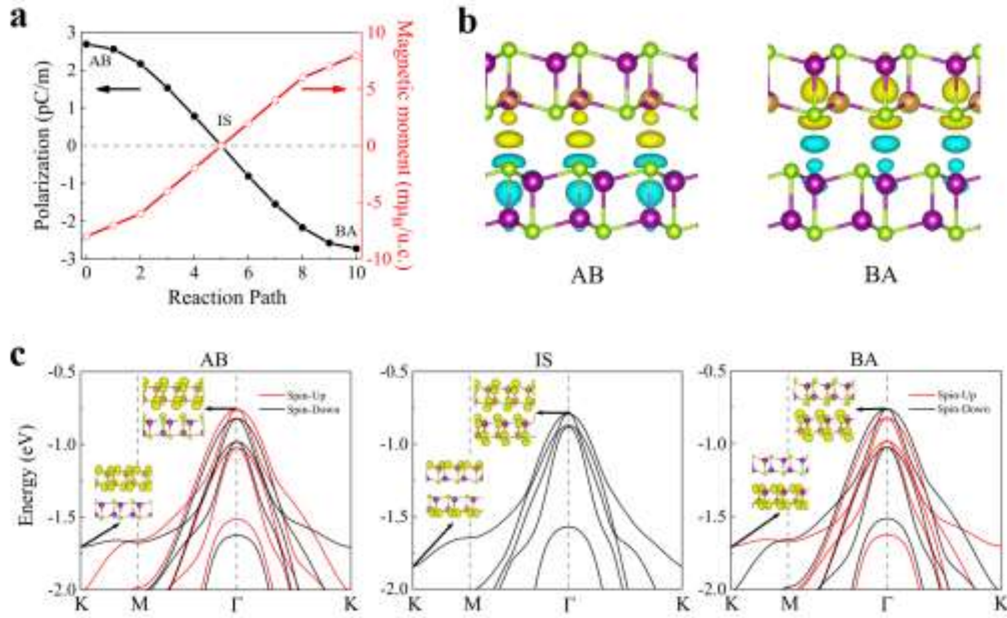

Fig. 3 Magnetoelectric coupling accompanied with electric polarization switching in MnSe bilayer. a Electric polarization and net magnetic moment variation as the interlayer sliding between AB and BA stacking in MnSe bilayer. **b** Spin density difference of AB, BA, in which the yellow and blue isosurfaces respectively indicate spin up/down electron accumulation/depletion and depletion/accumulation. **c** spin polarized band structure of AB, IS and BA. Insets are the partial charge density of highest occupied state in K and Γ.

The electric polarization and magnetoelectric coupling can be enhanced in MnSe trilayer and tetralayer, as shown in Fig. 4a, b. For the MnSe trilayer, we consider two energetically degenerate stacking patterns (ABA and BAB) with opposite electric polarization which are switchable via lateral sliding of the middle monolayer relative to the top and bottom monolayers. For MnSe tetralayer, the two switchable ferroelectric states have the stacking patterns of ABAB and BABA where the out-of-plane electric polarization can be reversed by the lateral sliding of the second and fourth monolayers. As shown in Supplementary Fig.2, the electric polarization of the MnSe trilayer and tetralayer are respectively 6.7 and 10.6 pC/m, which are larger than those of the MnSe bilayer. Particularly, the net magnetic moments are improved to 16 (trilayer) and 24

(tetralayer) mμ_B per unit cell, which are exactly twice and three times compared with MnSe bilayer, respectively, showing a linear relation of magnetoelectric coupling as the stacking number. The energy barriers for the lateral sliding are 12 (trilayer) and 13 (tetralayer) meV/f.u., respectively, which still lower than or comparable to most 2D ferroelectric material like In_2Se_3 (~ 60 meV/f.u.)[37], indicating the feasibility of vertical integration for nanoelectronics device.

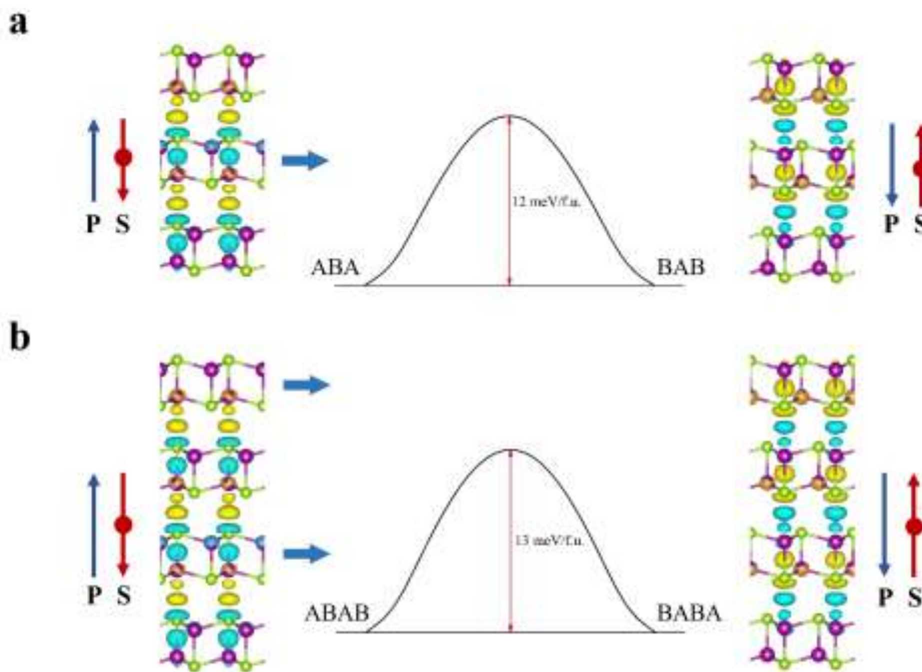

Fig. 4 Sliding ferroelectricity and magnetoelectric coupling in MnSe multilayer. a and **b** Ferroelectric switching pathway of MnSe trilayer and tetralayer, in which the ferroelectric switching barrier are marked by red double-sided arrow, and the orientation of ferroelectric polarization and net magnetic moments are respectively indicated by blue arrow and red arrow with centered circle.

3. **Magnetoelectric coupling tuned by external strain and/or hole doping**

The flexibility of 2D vdW materials enable significant response of electronic band structures to the external strain.[38] We therefore investigate the electric polarization and magnetoelectric coupling of MnSe bilayer under the compressive strain along the out-

of-plane direction and the biaxial in-plane tensile strain. The compressive strain along the out-of-plane direction can be quantized as the variation of the interlayer distance between top and bottom Se atom (d) relative to the equilibrium state (d_0), denoted as $\sigma_z = (d_0 - d)/d_0$. With the increase of compressive strain (decrease of interlayer distance), the interlayer coupling between the two monolayers is enhanced, which improves the electric polarization and net magnetic moment, as shown in Fig. 5a. At $\sigma_z = 0.1$, the electric potential difference between the two monolayers is improved to 0.39 eV and the net magnetic moment become 19 mμ_B per unit cell, which are about two times than those of the equilibrium state. This is accordance with the evolution of the electronic band structures. With the increase of compressive strain, the spin-splitting of the electronic bands increases, as shown in Supplementary Fig. 3a, which can be ascribed to the direct enhancement of hybridization of Mn and Se at the interface of MnSe bilayer along the out-of-plane direction.

The in-plane biaxial strain is defined as $\sigma_{x/y} = (a - a_0)/a_0$, where a and a_0 are the lattice constants of the strain and equilibrium states. With the increase of $\sigma_{x/y}$ (negative for compressive strain and positive for tensile strain), the electric polarization and magnetic moment are improved, as shown Fig. 5b. The compressive strain along the in-plane direction suppresses the electric polarization and the magnetoelectric coupling. In particular, the polarization and magnetic moment almost vanish when the compressive strain attains $\sigma_{x/y} = 0.1$. The in-plane tensile strain, however, enhances the electric polarization and magnetic moment. Moreover, the response of the electronic band structures to the tensile strain is quite remarkable, as shown in Supplementary Fig. 3b. The spin-splitting of the valence bands, especially in the region near the K point, increases with the increase of tensile. Moreover, the lowest conductance band energy

at the Γ point is reduced rapidly, making the strained MnSe bilayer be a direct-band-gap semiconductor as $\sigma_{x/y}$ ranging from 0.02 to 0.06.

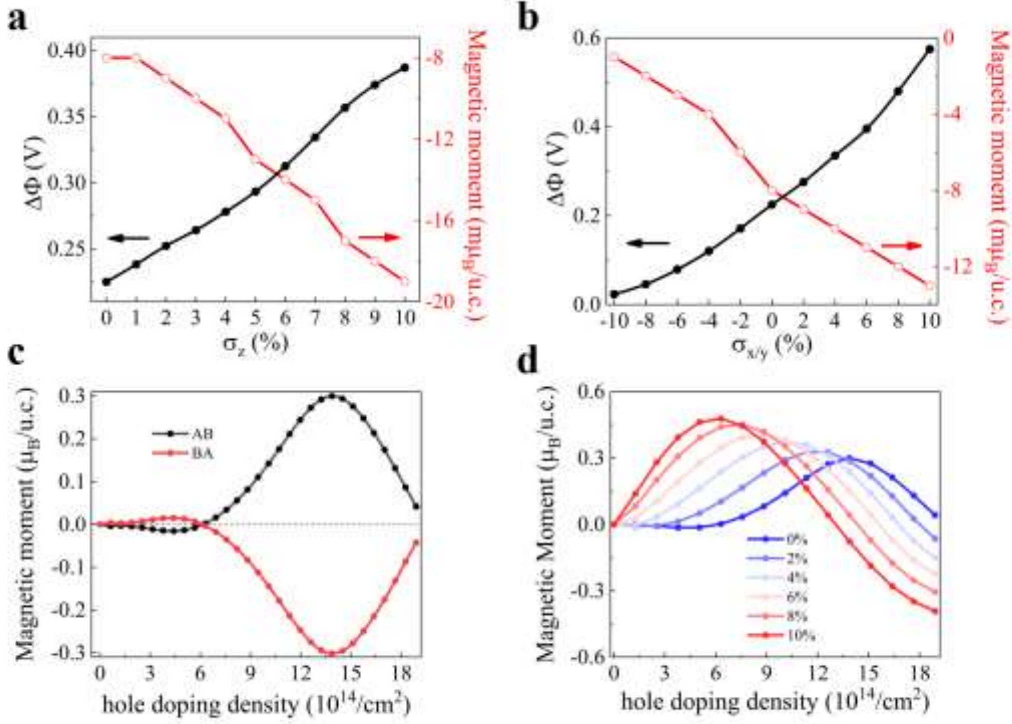

Fig. 5 Tunability of ferroelectricity and magnetoelectric coupling in MnSe bilayer. Variation of electric potential difference and net magnetic moment of AB stacking for MnSe bilayer as a function of **a** out-of-plane pressure and **b** biaxial in-plane strain. Hole doping dependence of net magnetic moment for **c** AB and BA stacking in MnSe bilayer and **d** AB stacking in MnSe bilayer under different biaxial tensile strain.

Electron or hole doping is also available for regulating the electric and magnetic properties of semiconductors. We therefore considered the variation of the magnetic moment of the MnSe bilayer in response to hole doping. For the AB stacking pattern, with the increase of hole doping concentration, the magnetism moments start to reach the negative maximum, then becomes positive rapidly, and reach the positive maximum (~ 0.3 μ_B/u.c.) at the hole doping concentration of 1.39×10^{15}/cm^2, as shown in Fig. 5c and Supplementary Fig. 4a. The MnSe bilayer with BA stacking pattern, the variation

of magnetic moment shows an opposite trend. This implies that the direction of the improved magnetic moment in the hole-doped MnSe bilayer can also be switched via lateral sliding between the two monolayer. Additionally, in view of the enhancement of magnetic moment due to the in-plane biaxial tensile strain, we further consider the synergistic effect of in-plane tensile strain and hole doping on the magnetic moment of MnSe bilayer. Our calculations revealed that maximal magnetic moment in the hole-doped MnSe bilayer under in-plane biaxial tensile are further improved and the corresponding hole-doping concentration is reduced compared with the unstrained MnSe bilayer, as shown in Fig. 5d. Under the biaxial tensile strain of $\sigma_{x/y} = 0.1$, the expected hole-doping concentration is decreased to $6.3 \times 10^{14}/cm^2$, which is attainable in experiment[39-41], as shown in Supplementary Fig. 4b. This offers a promising approach for enhancing the magnetoelectric coupling effect of the MnSe bilayer. More interestingly, the stacking-dependent multiferroicity of the MnSe bilayer enables tunable electric polarization and magnetic moire patterns by forming twisted MnSe bilayer, which is expected to open an avenue for study of 2D multiferroicity.

CONCLUSION

In summary, we demonstrate from first-principles calculations the newly-synthesized MnSe multilayers have SFE along with magnetoelectric effect in which both the electric polarization and magnet moment can be switched via lateral sliding between the monolayers. The electric polarization of MnSe bilayer is stronger than that of BN bilayer and can be further improved in MnSe trilayer and tetralayer. Moreover, the electric polarization and the corresponding magnetism can be enhanced by applying moderate out-of-plane compressive strain or biaxial in-plane tensile strain and/or hole doping. The moderate sliding energy barrier, switchable electric polarization and

magnetism suggest the promising potential of MnSe in multiferroic and spintronic applications.

METHODS

Our first-principles calculations within the density functional theory (DFT) were carried out using the Vienna Ab Initio Simulation Package (VASP) code[42,43]. The generalized gradient approximation in the Perdew-Burke-Ernzerhof (GGA-PBE) was adopted for the exchange-correlation functional[44] and the projector-augmented wave (PAW) pseudopotentials method[45] were applied to describe the interaction between the ions and valence electrons. The electron wavefunctions were expanded by a plane-wave basis with the kinetic energy cutoff of 500 eV. The DFT-D2 method of Grimme[46] was included to describe the van der Waals interaction. A large vacuum space up to 20 Å was set in the out-of-plane direction to avoid spurious interaction between images. The Brillouin zone (BZ) was sampled with Γ-centered 9×9×1 and 13×13×1 Monkhorst-Pack k mesh[47] for geometry optimization and electronic structure self-consistent calculations, respectively. The geometry structure was fully relaxed until the force on each atom is less than 0.01 eV/Å, and the electronic structure self-consistent convergence criteria was set to 10^{-7} eV. The GGA+U approach[48] with U_{eff} = 2.3 eV for 3d electron of Mn atom was used to treat on-site Coulomb interaction, which is reasonably validated in previous report[34]. The climbing image nudged elastic band (CINEB) method[49] was used to estimate the ferroelectric switching energy barrier, and the Berry phase approach[50, 51] was applied to evaluate the electric polarization.

DATA AVAILABILITY

The data that support the findings of this study are available in the paper and the Supplementary Information.

REFERENCES

1. Scott, J. F. Applications of modern ferroelectrics. *Science* **315**, 954-959 (2007).
2. Ghosez, P. & Rabe, K. M. Microscopic model of ferroelectricity in stress-free $PbTiO_3$ ultrathin films. *Appl. Phys. Lett.* **76**, 2767-2769 (2000).
3. Tenne, D. A. et al. Ferroelectricity in Ultrathin $BaTiO_3$ Films: Probing the Size Effect by Ultraviolet Raman Spectroscopy. *Phys. Rev. Lett.* **103,** 177601 (2009).
4. Ravindran, P., Vidya, R., Kjekshus, A., Fjellvag, H. & Eriksson, O. Theoretical investigation of magnetoelectric behavior in $BiFeO_3$. *Phys. Rev. B* **74,** 224412 (2006).
5. Seidel, J. et al. Conduction at domain walls in oxide multiferroics. *Nat. Mater.* **8**, 229-234 (2009).
6. Junquera, J. & Ghosez, P. Critical thickness for ferroelectricity in perovskite ultrathin films. *Nature* **422**, 506-509 (2003).
7. Duan, C. G., Sabirianov, R. F., Mei, W. N., Jaswal, S. S. & Tsymbal, E. Y. Interface effect on ferroelectricity at the nanoscale. *Nano Lett.* **6**, 483-487 (2006).
8. Chang, K. et al. Discovery of robust in-plane ferroelectricity in atomic-thick SnTe. *Science* **353**, 274-278 (2016).
9. Chang, K. et al. Microscopic Manipulation of Ferroelectric Domains in SnSe Monolayers at Room Temperature. *Nano Lett.* **20**, 6590-6597 (2020).
10. Higashitarumizu, N. et al. Purely in-plane ferroelectricity in monolayer SnS at room temperature. *Nat. Commun.* **11,** 2428 (2020).
11. Belianinov, A. et al. $CuInP_2S_6$ Room Temperature Layered Ferroelectric. *Nano Letters* **15**, 3808-3814 (2015).
12. Liu, F. C. et al. Room-temperature ferroelectricity in $CuInP_2S_6$ ultrathin flakes. *Nat. Commun.* **7,** (2016).
13. Zhou, Y. et al. Out-of-Plane Piezoelectricity and Ferroelectricity in Layered alpha-In_2Se_3 Nanoflakes. *Nano Lett.* **17**, 5508-5513 (2017).
14. Zheng, C. X. et al. Room temperature in-plane ferroelectricity in van der Waals In_2Se_3. *Sci. Adv.* **4,** eaar7720 (2018).
15. Wan, Y. et al. Room-Temperature Ferroelectricity in 1T'-ReS_2 Multilayers. *Phys. Rev. Lett.* **128,** 067601 (2022).
16. Wang, X. et al. Interfacial ferroelectricity in rhombohedral-stacked bilayer transition metal dichalcogenides. *Nat. Nanotechnol.* **17,** 367-371 (2022).
17. Weston, A. et al. Interfacial ferroelectricity in marginally twisted 2D semiconductors. *Nat. Nanotechnol.* **17,** 390-395 (2022).
18. Stern, M. V. et al. Interfacial ferroelectricity by van der Waals sliding. *Science* **372**, 1462-1466 (2021).
19. Woods, C. R. et al. Charge-polarized interfacial superlattices in marginally twisted hexagonal boron nitride. *Nat. Commun.* **12**, 347 (2021).

20. Yasuda, K., Wang, X. R., Watanabe, K., Taniguchi, T. & Jarillo-Herrero, P. Stacking-engineered ferroelectricity in bilayer boron nitride. *Science* **372**, 1458-1462 (2021).
21. Fei, Z. Y. et al. Ferroelectric switching of a two-dimensional metal. *Nature* **560**, 336-339 (2018).
22. Sharma, P. et al. A room-temperature ferroelectric semimetal. *Sci. Adv.* **5,** eaax5080 (2019).
23. Xiao, J. et al. Berry curvature memory through electrically driven stacking transitions. *Nat. Phys.* **16**, 1028-1034 (2020).
24. Rogee, L. et al. Ferroelectricity in untwisted heterobilayers of transition metal dichalcogenides. *Science* **376**, 973-978 (2022).
25. Li, L. & Wu, M. H. Binary Compound Bilayer and Multilayer with Vertical Polarizations: Two-Dimensional Ferroelectrics, Multiferroics, and Nanogenerators. *Acs Nano* **11**, 6382-6388 (2017).
26. Yang, Q., Wu, M. H. & Li, J. Origin of Two-Dimensional Vertical Ferroelectricity in WTe_2 Bilayer and Multilayer. *J. Phys. Chem. Lett.* **9**, 7160-7164 (2018).
27. Gao, Y. Y., Gao, M. Y. & Lu, Y. R. Two-dimensional multiferroics. *Nanoscale* **13**, 19324-19340 (2021).
28. Eerenstein, W., Mathur, N. D. & Scott, J. F. Multiferroic and magnetoelectric materials. *Nature* **442**, 759-765 (2006).
29. Fiebig, M., Lottermoser, T., Meier, D. & Trassin, M. The evolution of multiferroics. *Nat. Rev. Mater.* **1,** 16046 (2016).
30. Dong, S., Xiang, H. & Dagotto, E. Magnetoelectricity in multiferroics: a theoretical perspective. *Natl Sci. Rev.* **6**, 629-641 (2019).
31. Dong, S., Liu, J. M., Cheong, S. W. & Ren, Z. F. Multiferroic materials and magnetoelectric physics: symmetry, entanglement, excitation, and topology. *Adv. Phys.* **64**, 519-626 (2015).
32. Lu, C. L., Wu, M., Lin, L. & Liu, J. M. Single-phase multiferroics: new materials, phenomena, and physics. *Natl Sci. Rev.* **6**, 653-668 (2019).
33. Liu, X., Pyatakov, A. P. & Ren, W. Magnetoelectric Coupling in Multiferroic Bilayer VS_2. *Phys. Rev. Lett.* **125,** 247601 (2020).
34. Yan, H. et al. Electric-Field-Controlled Antiferromagnetic Spinctronic Devices. *Adv. Mater.* **32**, 1905603 (2020).
35. Aapro, M. et al. Synthesis and Properties of Monolayer MnSe with Unusual Atomic Structure and Antiferromagnetic Ordering. *ACS Nano* **15**, 13794-13802 (2021).
36. Lin, Z. Z., Si, C., Duan, S. R., Wang, C. & Duan, W. H. Rashba splitting in bilayer transition metal dichalcogenides controlled by electronic ferroelectricity. *Phys. Rev. B* **100,** 155408 (2019).
37. Ding, W. J. et al. Prediction of intrinsic two-dimensional ferroelectrics in In_2Se_3 and other III_2-VI_3 van der Waals materials. *Nat. Commun.* **8,** 14956 (2017).
38. Miao, F., Liang, S. J. & Cheng, B. Straintronics with van der Waals materials. *npj Quantum Mater.* **6,** 59 (2021).
39. Efetov, D. K. & Kim, P. Controlling Electron-Phonon Interactions in Graphene at Ultrahigh Carrier Densities. *Phys. Rev. Lett.* **105,** 256805 (2010).
40. Ye, J. T. et al. Accessing the transport properties of graphene and its multilayers at high carrier density. *Proc. Natl Acad. Sci. USA* **108**, 13002-13006 (2011).
41. Li, L. J. et al. Controlling many-body states by the electric-field effect in a two-dimensional material. *Nature* **529**, 185-189 (2016).
42. Kresse, G. & Hafner, J. AB initio molecular dynamics for open-shell transition metals. *Phys. Rev. B* **48**, 13115 (1993).

43. Kresse, G. & Furthmuller, J. Efficiency of ab-initio total energy calculations for metals and semiconductors using a plane-wave basis set. *Computational Mater. Sci.* **6**, 15-50 (1996).
44. Perdew, J. P., Burke, K. & Ernzerhof, M. Generalized gradient approximation made simple. *Phys. Rev. Lett.* **77**, 3865 (1996).
45. Kresse, G. & Joubert, D. From ultrasoft pseudopotentials to the projector augmented-wave method. *Phys. Rev. B* **59**, 1758 (1999).
46. Grimme, S. Semiempirical GGA-type density functional constructed with a long-range dispersion correction. *J. Comput. Chem.* **27**, 1787-1799 (2006).
47. Monkhorst, H. J. & Pack, J. D. Special points for Brillouin-zone integrations. *Phys. Rev. B* **13**, 5188 (1976).
48. Dudarev, S. L., Botton, G. A., Savrasov, S. Y., Humphreys, C. J. & Sutton, A. P. Electron-energy-loss spectra and the structural stability of nickel oxide: An LSDA+U study. *Phys. Rev. B* **57**, 1505 (1998).
49. Henkelman, G., Uberuaga, B. P. & Jonsson, H. A climbing image nudged elastic band method for finding saddle points and minimum energy paths. *J. Chem. Phys.* **113**, 9901-9904 (2000).
50. Kingsmith, R. D. & Vanderbilt, D. Theory of polarization of crystalline solids. *Phys. Rev. B* **47**, 1651(R) (1993).
51. Resta, R. Macroscopic polarization in crystalline dielectrics: the geometric phase approach. *Rev. Mod. Phys.* **66**, 899 (1994).

ACKNOWLEDGEMENTS

This work is supported by the National Natural Science Foundation of China (No. 12074218) and the Taishan Scholar Program of Shandong Province.

AUTHOR CONTRIBUTIONS

M.Z. conceived the project. K. L. and X.M. performed the first-principles calculations and conducted theoretical analysis. S. X. and Y.L. conducted the theoretical analysis. K. L. and M.Z. wrote the manuscript.

COMPETING INTERESTS

The authors declare no competing interests.

Supplementary Files

This is a list of supplementary files associated with this preprint. Click to download.

- SupplementaryMaterial.docx